Role of Fe in long-range ordered Ni_2Cr precipitates in Ni-Cr-Fe model alloys during isothermal aging

N. J. Aerne[1], D. J. Sprouster[2], J. D. Tucker[1,]*

[1] School of Mechanical, Industrial and Manufacturing Engineering, Oregon State University, Corvallis, OR 97331, USA

[2] Department of Materials Science and Chemical Engineering, Stony Brook University, Stony Brook, NY 11794, USA

**Julie.Tucker@oregonstate.edu*

Abstract

The precipitation of new phases during long-term service at elevated temperatures is a concern for the thermal stability of engineering alloys. In Ni-Cr-based alloys, *e.g., Alloy 690*, the formation of long-range ordered Ni_2Cr causes embrittlement and may impact the lifetime of nuclear power plant components. In this work, we quantify the formation and evolution of Ni_2Cr precipitation in eleven Ni-Cr-Fe model alloys with 0, 5, 7, and 10 wt. % Fe contents, and with Ni/Cr atomic ratios of 1.8, 2.0, 2.2, 2.4. These alloys were isothermally aged up to 10,000 h at temperatures between 330-475 °C. The alloys were characterized by synchrotron-based x-ray diffraction and Vickers hardness testing to quantify Ni_2Cr precipitate size, and the impact of precipitate size on the mechanical properties as a function of Fe content. After 10,000 h of aging at 475 °C and 418 °C, the formation of Ni_2Cr was observed in all alloys with 0 and 5 wt. % Fe. After 10,000 h of aging at 418 °C, Ni_2Cr precipitates were also observed in the 7 wt. % Fe containing Ni/Cr=2.0 sample. No clear evidence of Ni_2Cr was observed in any of the 10 wt. % Fe samples at any time and temperature combination. We find that the face-centered cubic matrix lattice contraction and Vickers hardness are correlated with the Ni_2Cr formation. The greatest change in hardness and lattice contraction occurs in stoichiometric alloys (Ni/Cr=2.0) with 0 wt. % Fe at 475 °C. The rate of change in the material properties for the 5 wt. % Fe alloys is reduced, however the magnitude of changes is similar to 0 wt. % Fe alloys. A precipitation hardening model developed for Ni-Cr alloys based on critical resolved shear stress with weakly coupled dislocations shows a clear link between Ni_2Cr precipitate size and hardness. This trend held across all alloys with Ni_2Cr formation regardless of Fe concentration. This important structure-property relationship can potentially help define Ni-Cr-Fe-based component lifetimes directly through an understanding of how Ni_2Cr formation impacts mechanical properties as a function of Fe content.

Keywords: *Nickel alloys, Long-range ordering, Hardness, Synchrotron diffraction, Precipitation strengthening, Critical resolved shear stress*

1. *Introduction*

High-strength and corrosion-resistance are intrinsic material properties that make Ni-based alloys attractive structural materials for the extreme environments of the nuclear power and other industries. However, license extensions for reactor operations beyond the initial 40 year time period raises concern for material integrity [1]. One particular concern for Ni-based alloys is the embrittlement from long-range order (LRO) phase transformations including those that occur after long time periods at elevated temperatures. This has prompted research into Ni-based alloy 690 (58-62 wt. % Ni, 27-31 wt. % Cr, 7-11 wt. % Fe, and minor alloying additions), a material used for steam generator tubing, baffles and replacement of other components of alloy 600 that operate in a temperature range of 270-325 °C [2]–[5]. In the Ni-Cr-Fe system, LRO phase formation of Ni_2Cr, and subsequent mechanical property changes after long-term isothermal aging at temperatures between 330-600 °C have been investigated by the global metallurgy community [4], [6]–[14]. Previous investigations have found that after 60,000 h of aging at 420 °C, LRO is observed in alloy 690 with 7 wt. % Fe, but not in 10 wt. % Fe. Further aging to 90,000 h at 360 °C showed no evidence of LRO in either the 7 or 10 wt. % [2]. These studies concluded that LRO would not be expected at 325 °C after 60 years in high Fe containing 690, while 690 with lower amounts may form [2]. However, there is limited data at lower temperatures and longer times of interest to industry.

The kinetics of long-range ordering in the Ni-Cr-Fe ternary alloys, the time-temperature-transformation diagram and phase diagram for Ni-Cr-Fe ternary alloys are less understood than the Ni-Cr binary system, especially at lower temperatures [6], [7], [9], [10]. Previous research suggests that increased Fe acts to lower the temperature at which the LRO phase is stable, however the activation energy does not appear to be influenced based on the limited available isothermal data [4], [15]. In model Ni-Cr binary alloys, LRO is readily found after 500 h of aging at 475 °C [10], [14], which is near the peak transformation temperature in these alloys. LRO in a ternary model alloys (59.4 at. % Ni, 30.2 at.% Cr, 10.4 at. % Fe) is observed after 32,000 h at 475 °C from changes in electrical resistivity, microhardness, and transmission electron microscopy (TEM), while above 500 °C the microhardness and lattice parameter variation were not observed [6], [7]. However, the critical temperature, the peak transformation temperature, and phase boundary of LRO for ternary alloys with respect to Fe content is less understood. Ni_2Cr phase formation was studied using proton irradiation in 12 commercial alloys with Fe contents ranging 2 to 50 wt. %. [16] LRO was found in alloy 690 (10.38 wt. % Fe) after irradiation to 2.5 dpa at 360 °C, indicating that Ni_2Cr is thermodynamically preferred, but kinetically constrained in purely thermal conditions. Alloys containing Fe contents higher than 18 wt. % showed no LRO [16]. This discrepancy between the rate of ordering of alloy 690 and comparable model alloys requires further research [16]. Furthermore, these previous studies highlight that there is still a need to systematically understand LRO as a function of composition to better explain differences between model binary, ternary, and commercial Ni-Cr-Fe alloys.

The formation of Ni_2Cr precipitates in Ni-Cr-Fe model and commercial alloys can take thousands of hours of isothermal aging and is dependent on temperature, composition, and material history. The most frequent technique used to gauge LRO is hardness testing [2], [5], [6], [8]–[10], [16] as LRO leads to measurable increases in hardness. However, other factors can contribute to material hardening (*i.e.* radiation, cold work, residual stress, other precipitates, grain orientation). Tensile data from a near stoichiometric (Ni/Cr=2.0) binary model alloy isothermally aged for 2000 h at 475 °C shows ductility loss compared to the as-received (AR) condition. Additionally, yield strength and hardness were found to correlate linearly [9]. Previous results from Ni-Cr binary model alloys (Ni/Cr=1.8, 2.0, 2.2, and 2.4) in [14] show evidence that the hardness and Ni_2Cr precipitate size correlate linearly and agree well with the critical resolved shear stress precipitation hardening model of weakly coupled dislocations. Thus, Ni_2Cr research that measures hardness or other properties are typically paired with a microstructure observation technique to confirm LRO is present in the materials.

Here, we quantify the structure-property relationship in a series of Ni-Cr-Fe ternary model alloys as functions of aging time, temperature, and composition. We focus on finding Ni_2Cr at lower temperatures and the connection between the model binary and ternary alloys comparable to commercial alloys with relevant Fe concentrations. Eleven Ni-Cr-Fe ternary model alloys of various stoichiometries (Ni/Cr = 1.8, 2.0, 2.2, 2.4) with 0, 5, 7, and 10 wt. % Fe were investigated following isothermal aging campaigns up to 10,000 h at four temperatures (330, 360, 418, and 475 °C) . The evolution in microstructure and mechanical properties were determined from synchrotron-based x-ray diffraction (XRD) and Vickers hardness testing, respectively. The evolution of the microstructure including the Ni-matrix face-centered cubic (FCC) lattice parameter, and the size of Ni_2Cr ordered precipitates were correlated with hardness data. These results serve to aid Ni-based alloy service life predictions at elevated temperatures by understanding the formation of LRO Ni_2Cr and mechanical property impacts in Ni-Cr-Fe ternary model alloys.

2. ***Experimental Methods***

2.1. Alloy Fabrication and Aging

The Ni-Cr-Fe ternary alloys were fabricated via vacuum induction melting and cast into an ~8 kg cylindrical ingot. All ingots were made from high purity raw materials and prepared with different stoichiometries for Ni/Cr atomic ratios from 1.8 to 2.4 with Fe content of 0, 5, 7, or 10 wt. %. Minor amounts of C were added for grain size control to better mimic commercial alloys. After casting, the ingot hot top was removed, and heat treated in a vacuum furnace, based on computationally optimized homogenization [17], [18], to reach a uniformity within 1 % of target composition. The ingots were then hot worked at approximately 900 °C into plate forms with a final thickness of ~16 mm through a series of forging and rolling operations, then air cooled to room temperature. The chemical composition of the ingot was verified through x-ray fluorescence and following ASTM E1621. The alloy compositions are given in Table 1. The rolled plates were then cut via electrical discharge machining into 12×12×16 mm^3 cuboid samples. The samples were then isothermally aged in box type furnaces at temperatures of 330, 360, 418, and 475 °C in air with aging times of 3,000 and 10,000 h, followed by furnace cooling to room temperature. Additional details on the temperature monitoring and calibration of the furnace system can be found in ref. [10]. The isothermal aging temperatures were maintained at ±5 °C of target temperatures, and the time accrued for aging campaigns are estimated to be ±1 % of target times.

Table 1. Chemical composition (wt. %) of alloys investigated.

Alloy Name: Letter + Target Ni-Cr Atomic ratio + wt. % Fe	Ni	Cr	Fe	Nb	Ti	Al	C	other*
A (Ni/Cr=1.8+0 Fe)	66.88	33.00	0	0.003	0.023	0.020	0.051	<0.023
K (Ni/Cr=1.8+5 Fe)	63.71	31.25	4.96	0.003	0.019	0.015	0.025	<0.018
M (Ni/Cr=1.8+10 Fe)	60.26	29.60	10.08	0.002	0.001	0.015	0.023	<0.019
B (Ni/Cr=2.0+0 Fe)	69.46	30.48	0	0.003	0.003	0.018	0.023	<0.013
F (Ni/Cr=2.0+5 Fe)	65.90	29.09	4.94	0.002	0.005	0.021	0.023	<0.019
G (Ni/Cr=2.0+7 Fe)	64.44	28.50	7.00	0.003	0.007	0.013	0.023	<0.014
H (Ni/Cr=2.0+10 Fe)	62.25	27.63	10.06	0.002	0.010	0.012	0.023	<0.013
C (Ni/Cr=2.2+0 Fe)	71.41	28.52	0	0.006	0.014	0.018	0.024	<0.008
J (Ni/Cr=2.2+5 Fe)	67.70	27.22	4.99	0.004	0.014	0.014	0.023	<0.035
L (Ni/Cr=2.2+10 Fe)	64.03	25.82	10.07	0.003	0.009	0.012	0.024	<0.032
D (Ni/Cr=2.4+0 Fe)	73.05	26.86	0	0.002	<0.001	0.047	0.023	<0.017

other*- P <0.001: Cu, Mn, Si, Co, Mo, W, Ta, V <0.010

Optical microscopy images of alloys B (Ni/Cr=2.0+0 Fe) and H (Ni/Cr=2.0+10 Fe) after aging for 10,000 h at 475 °C are shown in Figure 1. The surface was polished as described in the hardness testing section and then etched with waterless Kailing #2 solution for 10-30 s to reveal the grain structure. Alloy B etched with less time than the alloy H. The Abrams three circle procedure was applied to compare the grain size [19], [20]. No significant difference between average grain size is observed and the average grain size of the alloys is 29±8 microns.

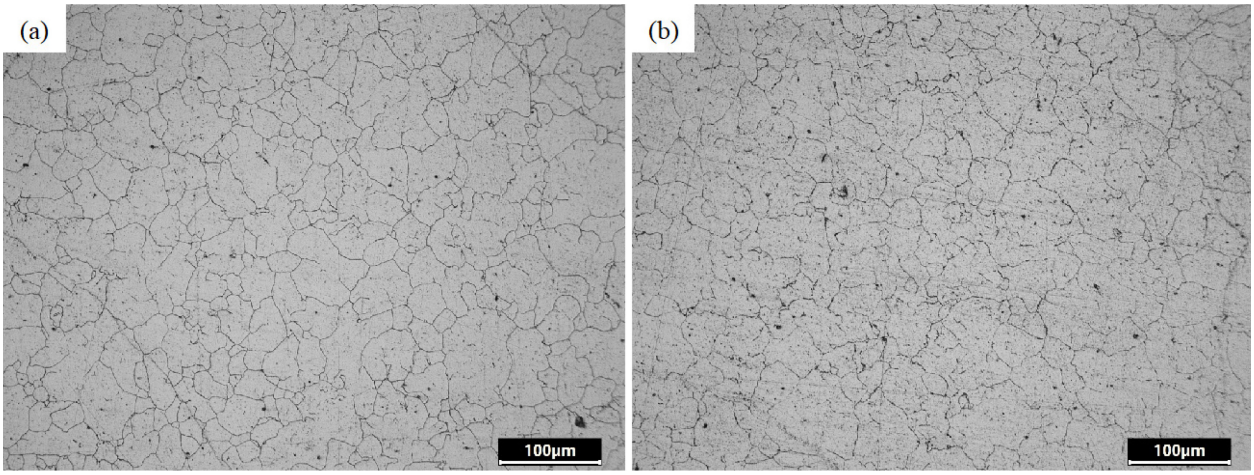

Figure 1. Optical micrographs for (a) alloy B (Ni/Cr=2.0+0 Fe) and (b) alloy H (Ni/Cr=2.0+10 Fe) after isothermal aging at 475°C after 10,000 h.

2.2. Hardness testing

Vickers hardness testing was performed on a top side of the cuboid samples, *i.e.,* the plate face. The surface finish for testing was achieved via wet polishing on standard 8-inch polishing wheels using SiC (240 to 1,200 grit), and then using alumina polishing solutions from 1 μm to 0.05 μm on felt polishing pads. Hardness measurements were performed using a Leco 400 A hardness tester with pyramidal diamond tip and a load of 500 gf (or 4.9 N) applied for 15 s. An M55× objective lens with a 0.65 numerical aperture was used to measure the diagonals of the residual imprints. Ten indentations were performed at independent locations on each sample following standard procedures for microhardness testing. The number of indents selected follows statistical analysis procedures of Vickers hardness research [21]. There were two independent cuboid samples from each condition for a total of twenty indents per condition. The average standard deviation of Vickers hardness values for all samples was ±7.3 HV.

2.3. X-ray diffraction (XRD)

Samples for XRD measurements were cut with electrical discharge machining from the side of cuboid samples to 5 × 5 × 0.1 mm^3 in size and mechanically polished. XRD measurements were performed at the Pair Distribution Function beamline 28-ID-1 [22], [23] at the National Synchrotron Light Source II. All samples were measured in transmission-mode geometry with an amorphous silicon-based flat panel detector. The sample-to-detector distance was calculated to be 1078.65 mm. The incident wavelength and of the x-ray beam was 0.1665 Å (74.47 keV). The samples were subject to a grid array for measurements to improve powder averaging. Count times for each pattern were 0.1 s with 600 individual frames collected from the grid array for a total exposure of 60 s per sample condition. These individual frames are then averaged together. A single dark image [600, 0.1 s exposures] was taken before the data collection of each sample. The sample-to-detector distance, tilts of the detector relative to the beam were determined using a LaB_6 NIST powder standard (reference material 660c). The two-dimensional detector images were radially integrated, and background subtracted to obtain powder diffraction patterns for refinement. Following standard refinement practices for polycrystalline materials. These operations were completed with the NIKA and IRENA programs [24], [25].

Refinements of the one-dimensional powder diffraction patterns were performed in MAUD [26]. The XRD peak profiles were modeled using a modified pseudo-Voigt function. The instrument contribution to the broadening of the measured profiles was quantified by fitting the LaB_6 powder standard, with known crystalline-domain size and negligible strain contribution. The Gaussian and Lorentzian-based broadening parameters were subsequently fixed during the analysis of the alloys under investigation. The precipitate sizes, and lattice parameters were allowed to vary during the refinements for the FCC matrix and Ni_2Cr. The weight fractions of Ni_2Cr precipitate phase were initially allowed to refine and were subsequently fixed to 9.0 % after minor variability from this refined value was found, consistent with weight fractions quantified in Ni-Cr binary alloys in ref. [14]. The microstrain parameter was allowed to be refined for the FCC host only (thus, the refined precipitate size parameters are lower limits for the Ni_2Cr phase). The 3,000 and 10,000 h specimens were selected to enhance and compliment results and discussion of available TEM literature on Ni_2Cr helping to collaborate our results with previous observations in comparable alloys [5], [9], [10]. The Ni/Cr stoichiometric atomic ratios (Ni/Cr=1.8, 2.0, 2.2, 2.4) with Fe compositions will help to understand the evolution of Ni_2Cr as a function of composition. The temperatures selected for the experiment serve to both bridge relevant industry conditions with key results of previous literature, i.e., other long term isothermal experiments of Ni-based alloys [2], [6]. This research covers 99 XRD measurements across the 11 Ni-Cr-Fe ternary model alloy compositions at 4 temperatures (330, 360, 418, 475 °C) and 3 times (0, 3,000, 10,000 h).

3. ***Results***

In section (3.1), the qualitative XRD results are discussed for stoichiometric alloys B, F, G, and H (Ni/Cr=2.0+0, 5, 7, 10 Fe) in the AR condition and after 10,000 h aging at temperatures between 330-475 °C. The off-stoichiometric alloys A, K, and M (Ni/Cr=1.8+0, 5, 10) and C, J, and L (Ni/Cr=2.2+0, 5, 10) XRD patterns are also shown. In section (3.2) the quantitative microstructural results from the XRD refinements are discussed together with the hardness results for stoichiometric alloys with various Fe contents alloys B, F, G, and H (Ni/Cr=2.0+0, 5, 7, 10). In section (3.3) the quantitative results for the off-stoichiometric alloys A, K, and M (Ni/Cr=1.8+0, 5, 10) and C, J, and L (Ni/Cr=2.2+0, 5, 10) are presented. Any samples not discussed in the text are presented in the supplemental materials section. The results for the AR specimen FCC matrix lattice parameters and hardness values are listed in Table 2. The alloys with notable Ni_2Cr formation are also given in Table 2 along with their Ni_2Cr precipitate size. The complete table of sample data is given in the supplementary materials section. The symbols in the figures of the result section use a circle for 0 wt. % Fe, a downward triangle for 5 wt. % Fe, an upward triangle for 7 wt. % Fe, and a square for 10 wt. % Fe.

Table 2. Summary of AR samples and select Ni-Cr-Fe model alloys: FCC matrix lattice parameter, Ni_2Cr precipitate size (if detected) and hardness.

Name	Temp °C	Time hr.	Lattice parameter Å ±	Precipitate-size nm ±	Hardness Value HV± std
A (Ni/Cr=1.8+0 Fe)	AR	-	3.55651 (0.00004)	-	188.4 (4.5)
B (Ni/Cr=2.0+0 Fe)	AR	-	3.55282 (0.00007)	-	180.1 (6.3)
C (Ni/Cr=2.2+0 Fe)	AR	-	3.54998 (0.00004)	-	184.0 (5.1)
D (Ni/Cr=2.4+0 Fe)	AR	-	3.54669 (0.00005)	-	177.3 (5.5)
K (Ni/Cr=1.8+5 Fe)	AR	-	3.55775 (0.00005)	-	183.0 (4.1)
F (Ni/Cr=2.0+5 Fe)	AR	-	3.55639 (0.00004)	-	184.4 (5.4)
J (Ni/Cr=2.2+5 Fe)	AR	-	3.55148 (0.00014)	-	178.1 (4.4)
G (Ni/Cr=2.0+7 Fe)	AR	-	3.55687 (0.00005)	-	176.7 (5.3)
M (Ni/Cr=1.8+10 Fe)	AR	-	3.55881 (0.00004)	-	179.0 (6.2)
H (Ni/Cr=2.0+10 Fe)	AR	-	3.55848 (0.00005)	-	173.0 (3.4)
L (Ni/Cr=2.2+10 Fe)	AR	-	3.55652 (0.00006)	-	177.3 (5.5)
A (Ni/Cr=1.8+5 Fe)	418	3000	3.55535 (0.00003)	3.9 (1.0)	231.2 (10.7)
A (Ni/Cr=1.8+5 Fe)	418	10000	3.54907 (0.00007)	15.9 (2.4)	344.5 (20.2)
B (Ni/Cr=2.0+5 Fe)	418	3000	3.55034 (0.00012)	5.7 (1.7)	241.3 (7.4)
B (Ni/Cr=2.0+5 Fe)	418	10000	3.54575 (0.00004)	12.8 (0.9)	295.0 (13.7)
C (Ni/Cr=2.2+5 Fe)	418	3000	3.54765 (0.00004)	6.3 (0.5)	244.7 (11.1)
C (Ni/Cr=2.2+5 Fe)	418	10000	3.54577 (0.00004)	9.1 (1.2)	277.6 (13.2)
D (Ni/Cr=2.4+0 Fe)	418	3000	3.54546 (0.00011)	6.3 (0.8)	235.7 (10.0)
D (Ni/Cr=2.4+0 Fe)	418	10000	3.54399 (0.00005)	8.9 (0.7)	255.7 (8.0)
K (Ni/Cr=1.8+5 Fe)	418	10000	3.55578 (0.00004)	4.1 (0.5)	225.9 (13.8)
F (Ni/Cr=2.0+5 Fe)	418	10000	3.55168 (0.00003)	7.9 (0.5)	254.2 (8.2)
J (Ni/Cr=2.2+5 Fe)	418	10000	3.54758 (0.00004)	7.6 (1.1)	240.3 (10.0)
G (Ni/Cr=2.0+7 Fe)	418	10000	3.55500 (0.00003)	3.9 (0.7)	212.8 (4.9)
A (Ni/Cr=1.8+0 Fe)	475	3000	3.55172 (0.00003)	13.2 (0.8)	317.5 (10.0)
A (Ni/Cr=1.8+0 Fe)	475	10000	3.54955 (0.00005)	15.0 (0.6)	334.2 (16.6)
B (Ni/Cr=2.0+0 Fe)	475	3000	3.54576 (0.00003)	15.4 (0.9)	315.8 (15.5)
B (Ni/Cr=2.0+0 Fe)	475	10000	3.54415 (0.00004)	16.3 (0.7)	334.1 (14.0)
C (Ni/Cr=2.2+0 Fe)	475	3000	3.54411 (0.00003)	11.9 (1.1)	298.2 (11.7)
C (Ni/Cr=2.2+0 Fe)	475	10000	3.54385 (0.00004)	14.3 (0.7)	319.9 (11.3)
D (Ni/Cr=2.4+0 Fe)	475	3000	3.54260 (0.00004)	10.9 (0.9)	281.2 (8.2)
D (Ni/Cr=2.4+0 Fe)	475	10000	3.54280 (0.00004)	11.6 (0.7)	293.6 (9.1)
K (Ni/Cr=1.8+5 Fe)	475	3000	3.55694 (0.00005)	4.4 (1.2)	216.2 (7.3)
K (Ni/Cr=1.8+5 Fe)	475	10000	3.55195 (0.00004)	14.7 (0.6)	328.7 (7.9)
F (Ni/Cr=2.0+5 Fe)	475	3000	3.55477 (0.00004)	10.9 (0.9)	281.2 (8.2)
F (Ni/Cr=2.0+5 Fe)	475	10000	3.54957 (0.00004)	12.2 (0.9)	313.9 (22.7)
J (Ni/Cr=2.2+5 Fe)	475	3000	3.54830 (0.00003)	8.5 (1.2)	267.9 (8.2)
J (Ni/Cr=2.2+5 Fe)	475	10000	3.54517 (0.00004)	14.6 (1.0)	312.6 (10.7)

3.1. Qualitative XRD analysis

The XRD patterns for the Ni-Cr-Fe model alloys are shown Figure 2 for the stoichiometric AR and aged samples after 10,000 h at 330-475 °C. Patterns are offset as functions of temperature to show the effects of increased Fe. The FCC matrix is labeled for reference. No alloy in the AR condition show LRO Ni_2Cr peaks. The body-centered orthorhombic Ni_2Cr phase precipitates are observable at lower two theta angles before the (111) and between the (200) and (220) matrix peaks. In Figure 2 (a) the LRO Ni_2Cr peaks are labeled for reference. These peak locations give the best qualitative results for clear LRO identification and are extensively used in quantitative refinement of the Ni_2Cr phase. No body-centered cubic Cr peaks were observed in any alloy. The XRD patterns for the Ni-Cr-Fe model alloys are shown in Figure 3 for the off-stoichiometric AR and aged samples after 10,000 h at 330-475 °C. Patterns are offset as functions of temperature to show the effects of increased Fe.

In Figure 2 (a) the XRD patterns for alloy B (Ni/Cr=2.0+0 Fe) show Ni_2Cr peaks at both 418 and 475 °C after 10,000 h. In Figure 2 (b) the XRD patterns for alloy F (Ni/Cr=2.0+5 Fe) show Ni_2Cr peaks at 418 and 475 °C after 10,000 h. In Figure 2 (c) the XRD patterns for alloy G (Ni/Cr=2.0+7 Fe) show early formation of Ni_2Cr at 418 °C after 10,000 h but not at 475 °C. In Figure 2 (d) the XRD patterns for alloy H (Ni/Cr=2.0+10 Fe) do not show Ni_2Cr peaks at any temperature. In Figure 3, the results for alloys A, K, and M (Ni/Cr=1.8+0, 5, 10 Fe), and C, J, and L (Ni/Cr=2.2+0, 5, 10 Fe) are similar to those of the stoichiometric alloy with similar Fe content. The alloy D (Ni/Cr=2.4+0 Fe) is shown in the supplemental materials section. The absence of distinct Ni_2Cr peaks at the lower temperatures of 330 and 360 °C across all alloys is indicative of sluggish kinetics, and the formation after longer periods should not be ruled out. The exception to this are the hypo-stoichiometric alloy A (Ni/Cr=1.8+0 Fe) which does show Ni_2Cr peaks as shown in Figure 3 (b). These results show that increased Fe content acts to slow the kinetics, as the formation with 5 wt. % Fe is less developed compared to the 0 wt. % Fe alloys at the same temperature. Visually identifying the Ni_2Cr peaks in alloy G (Ni/Cr=2.0 + 7 Fe) at 418 °C, but not at 475 °C show evidence that the critical temperature is depressed with increased Fe content. These results show that increased Fe content either slows the formation, and/or lowers the critical temperature for Ni_2Cr formation.

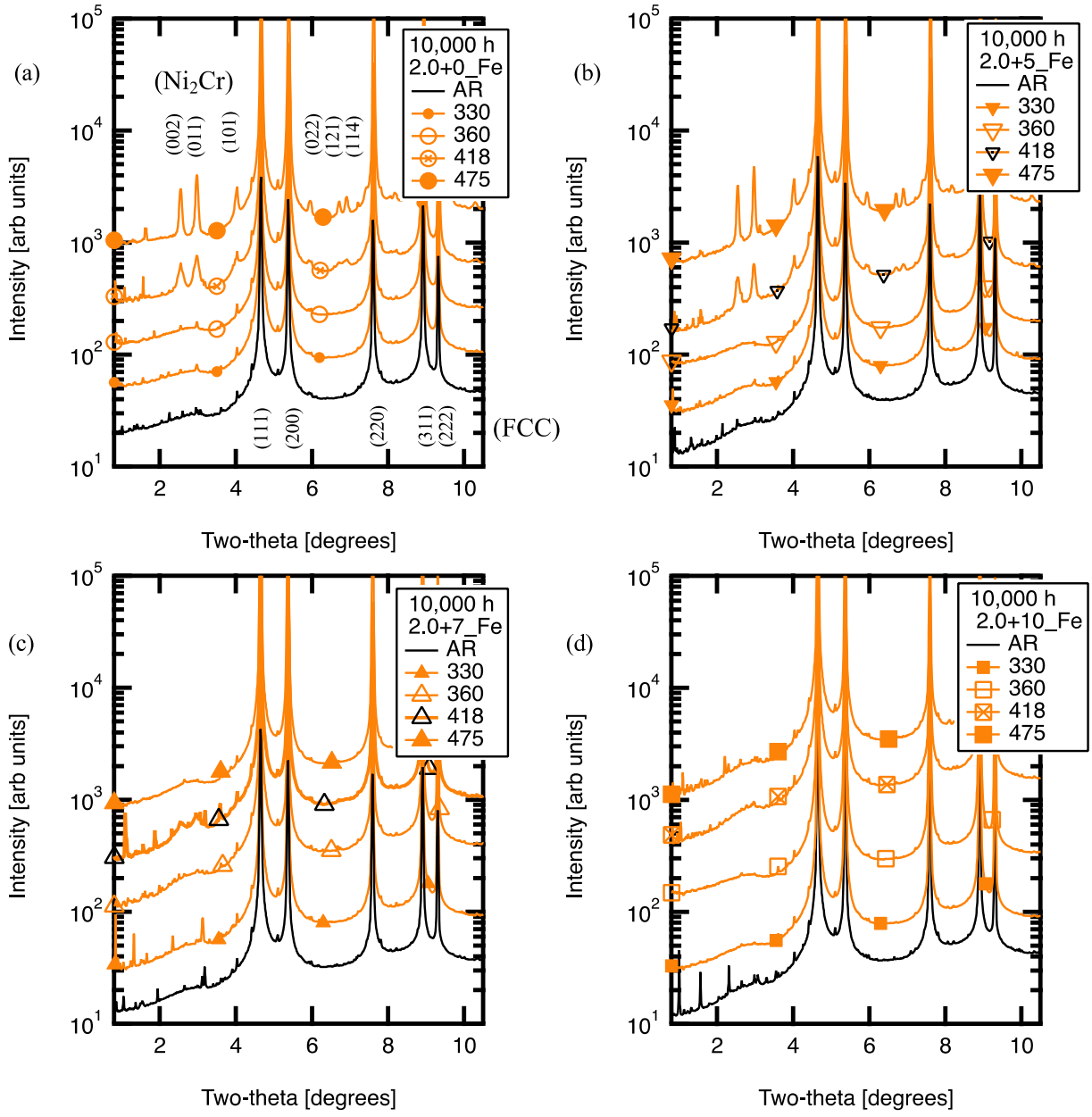

Figure 2 –XRD patterns for stoichiometric alloys after isothermal aging for 10,000 h at 330, 360, 418, 475 °C for alloy (a) B (Ni/Cr=2.0+0 Fe), (b) F (Ni/Cr=2.0+ 5 Fe), (c) G (Ni/Cr=2.0+ 7 Fe), (d) H (Ni/Cr=2.0+ 10 Fe). FCC peaks and Ni_2Cr peaks are labelled for reference in panel (a).

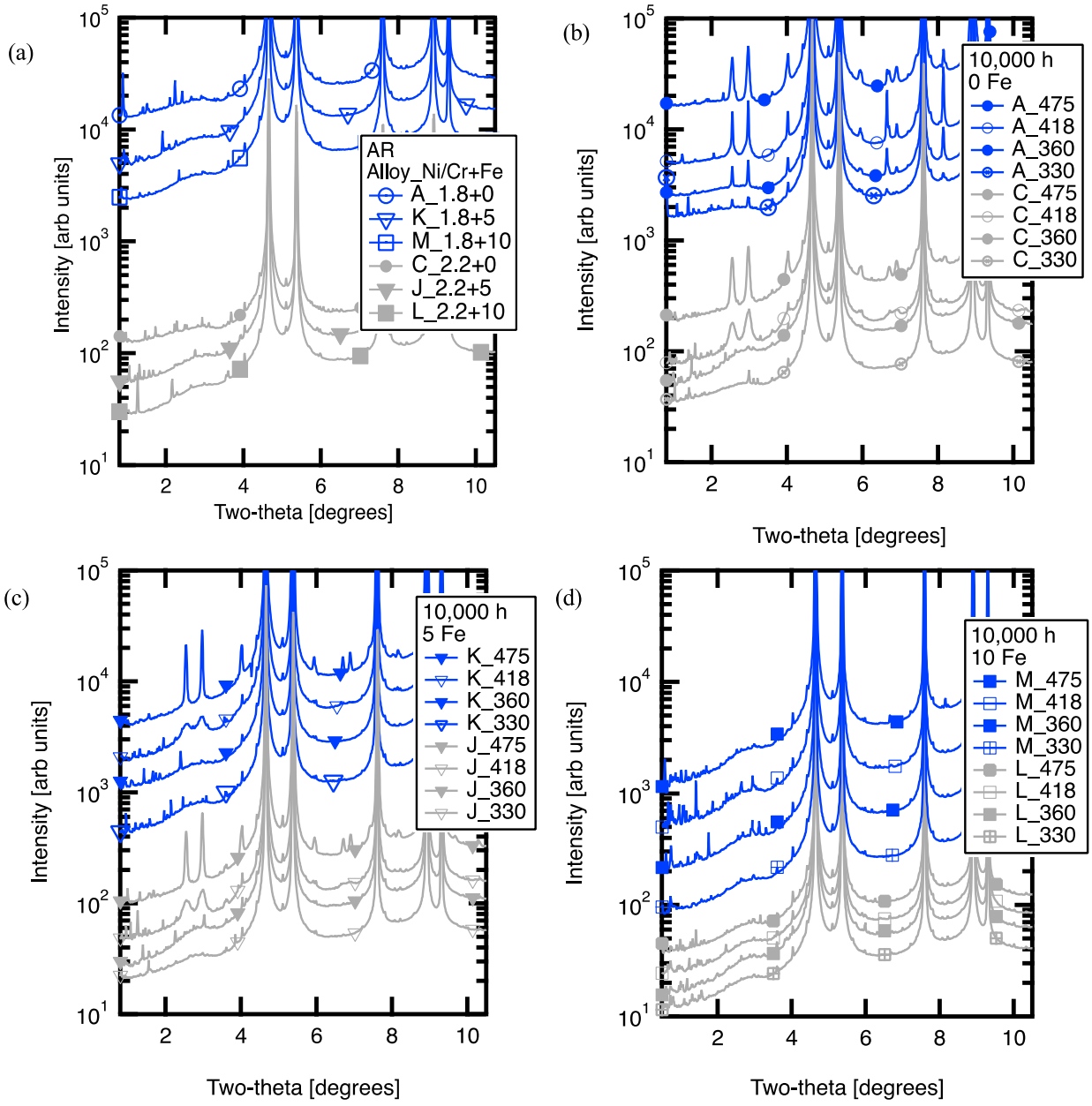

Figure 3 - XRD patterns for off-stoichiometric alloys in (a) AR condition for alloys A, K, and M (Ni/Cr=1.8 + 0, 5, and 10 Fe) and C, J, and L (Ni/Cr=2.2 + 0, 5, and 10 Fe), and (b)-(d) after isothermal aging for 10,000 h at 330, 360, 418, 475 °C. After aging 10,000 hours (b) shows alloys A (Ni/Cr=1.8 + 0 Fe) and C (Ni/Cr=2.2 + 0 Fe), (c) shows alloys K (Ni/Cr=1.8 + 5 Fe) and J (Ni/Cr=2.2 + 5 Fe), and (d) shows alloys M (Ni/Cr=1.8 + 10 Fe) and L (Ni/Cr=2.2 + 10 Fe).

3.2. Quantitative XRD results and hardness testing for stoichiometric alloys

The quantitative results from the XRD refinements and Vickers hardness testing for stoichiometric alloys are discussed in this section. Figure 4 shows the results for the FCC matrix lattice parameter and Vickers hardness after 3,000 and 10,000 h of aging at temperatures between 330-475 °C relative to the change in material property from the respective AR alloy. Both the FCC lattice parameter and Vickers hardness testing show changes occur after isothermal aging.

The greatest lattice contractions and change in hardness are quantified at the isothermal aging temperature 475 °C for stoichiometric alloy B (Ni/Cr=2.0+0 Fe). Alloy F (Ni/Cr=2.0+5 Fe) has the next largest amount of material property change after 10,000 h. The stoichiometric alloys with 7 and 10 wt. % Fe change less than the lower Fe containing alloys, with minor change in FCC matrix lattice parameter and no change in hardness at 475 °C. Alloy H (Ni/Cr=2.0+10 Fe) shows only marginal change in the matrix lattice parameter at each temperature and do not show notable change in hardness.

Across the compositions investigated here, there is less total change in the lattice parameters and hardness at 418 °C compared to 475 °C at both 3,000 and 10,000 h. At 330 and 360 °C there is less change across the stoichiometric alloys. After 3,000 h there is a noticeable difference in the formation between 0 and 5 wt. % Fe alloys in the stoichiometric alloys with the 0 wt. % Fe alloys having greater change in material property. The FCC matrix lattice parameter at 330 and 360 °C after 3,000 h shows some degree of variation across the compositions, which is potentially due to short-range order (SRO). In Figure 1 (a) the structure of alloy B (Ni/Cr=2.0+0 Fe) and Figure 1 (b) alloy H (Ni/Cr=2.0 +10 Fe) are shown after aging at 475 °C for 10,000 h. The similarities in grain size reveals that the difference in hardness are not attributed to grain boundary strengthening, recrystallization, *etc.*

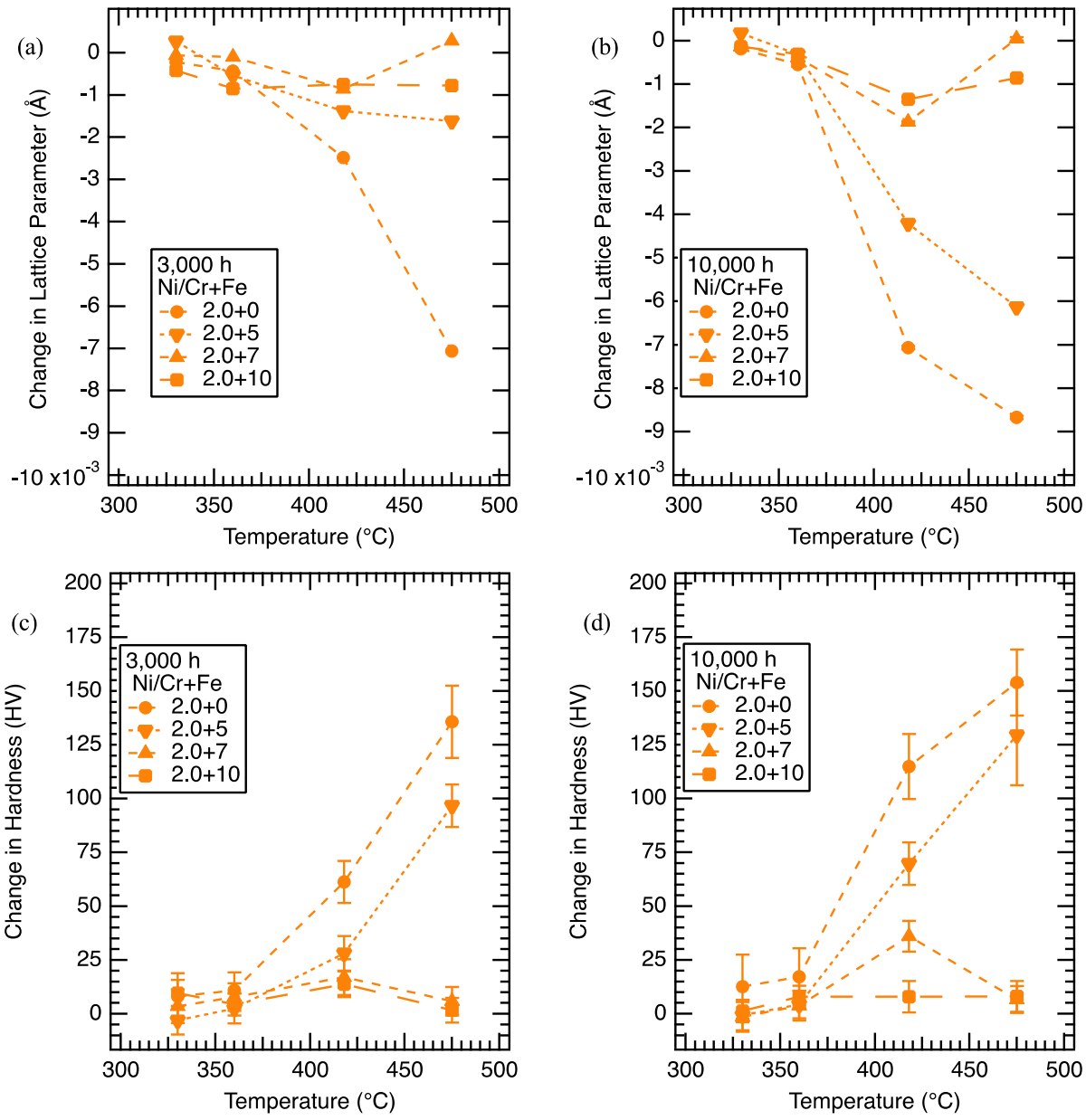

Figure 4- Quantitative XRD lattice parameters and hardness results for stoichiometric alloys. In Figure 4 (a) and (b) the lattice contraction from stoichiometric alloys after isothermal aging for 3,000 and 10,000 h at temperatures 330-475 °C are shown, respectively. In Figure 4 (c) and (d) the change in hardness from 3,000 and 10,000 h, respectively. Each figure shows only the stoichiometric (Ni/Cr=2.0) alloys with all Fe contents 0, 5, 7, and 10 wt. % Fe, alloys B, F, G, and H, respectively.

3.3. Quantitative XRD results and hardness testing for off-stoichiometric alloys

The quantitative results from the synchrotron XRD refinements and Vickers microhardness for off-stoichiometric alloys are presented in this section. Figure 5 shows the FCC matrix lattice parameter and Vickers hardness testing after 3,000 and 10,000 h at temperatures between 330-475 °C, relative to the change in material property from the AR alloys. Like the stoichiometric results in section 3.2, the off-stoichiometric alloys show significant changes occur after isothermal aging.

The quantitative changes in the FCC matrix lattice parameter and hardness show that after 10,000 hours of isothermal aging at 418 °C or 475 °C, alloy A (Ni/Cr=1.8+0 Fe) has the greatest change followed by alloy C (Ni/Cr=2.2 + 0 Fe). However, at 360 and 418 °C alloy A (Ni/Cr=1.8+0 Fe) has a notable increase over alloy C (Ni/Cr=2.2 +0 Fe). Following the 0 wt. % Fe alloys, alloy K (Ni/Cr=1.8 +5 Fe) and J (Ni/Cr=2.2+5 Fe) have the next largest amount of material property change after 10,000 h. Across the compositions there is less total changes at 418 °C compared to 475 °C at both 3,000 and 10,000 h. However, after 3,000 h there is a noticeable difference in the formation between 0 and 5 wt. % Fe alloys. Figure 5 shows the 0 wt. % Fe alloys have the greatest change in material properties. At the isothermal aging temperature 330 and 360 °C there is less change across the off-stoichiometric alloys. The 10 wt. % Fe alloys show only marginal change in the FCC matrix lattice parameter and do not show significant change in hardness at each temperature. The FCC matrix lattice parameter at 330 and 360 °C after 3,000 h again shows some degree of variation for the off-stoichiometric alloys, which may be signs of SRO as opposed to experimental scatter, or error.

The quantitative XRD and hardness results across the composition, time and temperatures show that isothermal aging for extended periods of time promote changes in the material properties. As the aging time increases from 3,000 to 10,000 h there is an increase in hardness and contraction in the FCC matrix lattice parameter at each temperature. However, the lower isothermal aging temperature of 418 °C has a larger change between aging times than 475 °C. Across the compositions there is less total change at 418 °C in comparison to 475 °C at both 3,000 and 10,000 h with the exception being the A (Ni/Cr=1.8+0 Fe) alloys, which changes slightly more at 418 °C after 10,000 h. The hypo-stoichiometric alloy A (Ni/Cr=1.8) has a significant change in hardness after 10,000 h at both 330 °C and 360 °C. Increasing Fe from 0 to 5 wt.% has a substantial impact on the contraction of hypo-stoichiometric alloys as observed in both the FCC matrix lattice contraction and change in hardness.

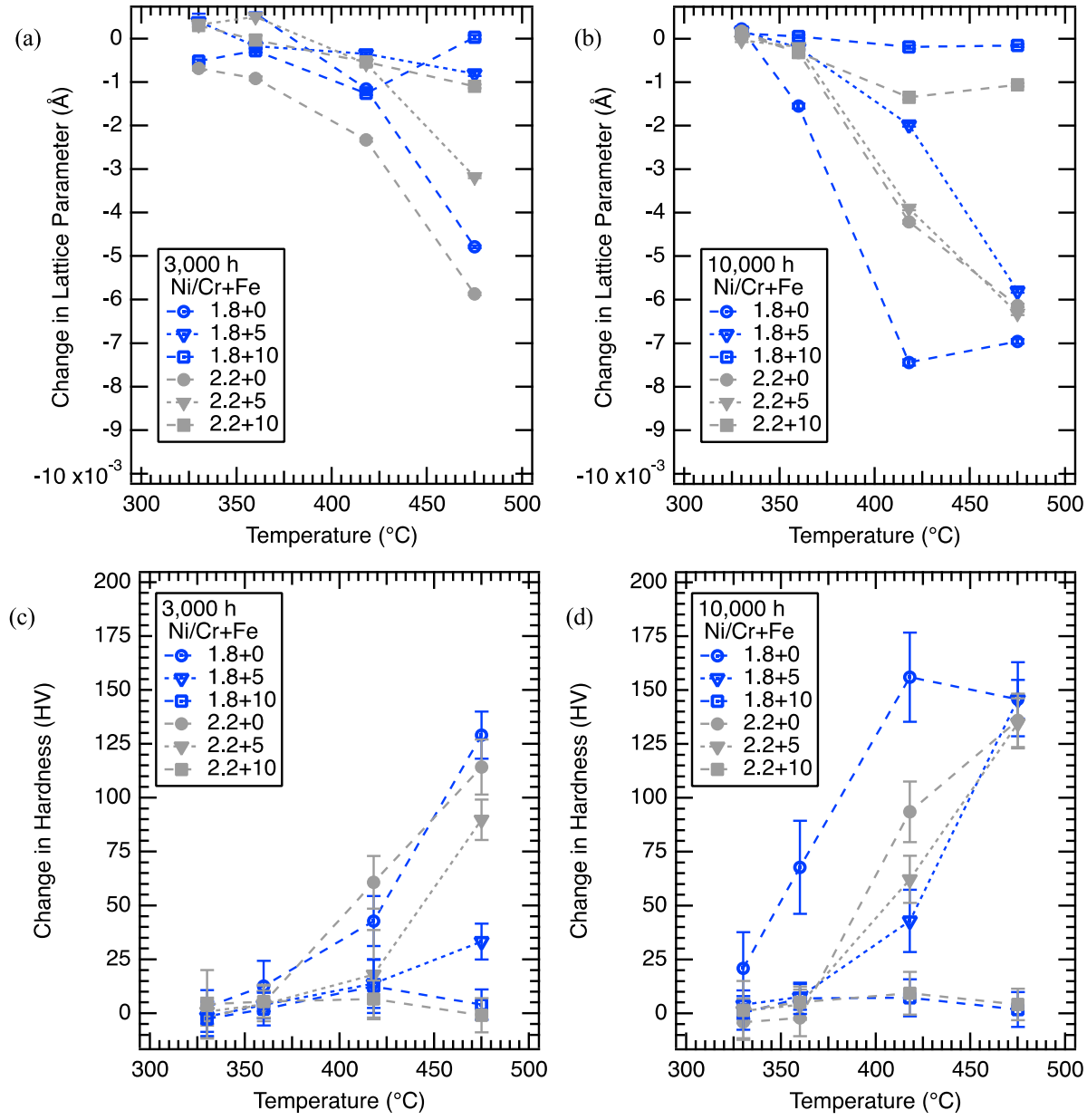

Figure 5 – Quantitative XRD and hardness results for off-stoichiometric alloys Ni/Cr = 1.8 and 2.2. Figures 5 (a) and (b) show the lattice contraction from 3,000 and 10,000 h of aging, respectively. Figures 5 (c) and (d) show the change in hardness from 3,000 and 10,000 h of aging, respectively. Each figure shows the off-stoichiometric alloys A, K, and M (Ni/Cr=1.8+ 0,5,10 Fe), blue open symbol, and C, J, and L (Ni/Cr=2.2+ 0, 5, 10 Fe), gray closed symbols.

4. Discussion

4.1. Agreement between quantitative analysis and previous literature

In section 3 above we show that when Ni_2Cr peaks are observed in XRD patterns, there is a concomitant change in the FCC matrix lattice parameter and hardness. Our findings show that Ni_2Cr precipitates are observable after a change of ~30 HV, or a 0.06 % change in the FCC matrix lattice parameter. At this degree of formation, Ni_2Cr precipitates are 3-5 nm in size. Sharper Ni_2Cr peaks are observed with even higher changes in hardness (~60 HV) and larger lattice contractions (0.08 to 0.11 %) depending on the composition. At this more developed stage, the Ni_2Cr precipitates are 6-9 nm in size. The Ni_2Cr peaks continue to develop with both increased time and temperature indicating further increases in Ni_2Cr precipitates size. Similar development was noted in ref. [9], where an increase in precipitate size was observed with TEM from 3,000 to 10,000 h. We find that above a change of 100 HV, or around 0.19 to 0.23% lattice contraction, Ni_2Cr precipitates have sizes in excess on ≥10 nm. Prior to Ni_2Cr precipitate formation, there are likely regions of SRO that act as nucleation sites for Ni_2Cr formation. These results are in agreement with ref. [9] where a lattice parameter contraction of 0.05% was coincident with the formation of Ni_2Cr precipitate formation for near (Ni/Cr=2.0) alloys. These last observations highlight the ability of synchrotron XRD to confirm the presence of LRO Ni_2Cr in early formation.

Table 2 shows that the FCC matrix lattice parameter and hardness in the AR conditions are dependent on the composition of Ni, Cr, and Fe. The AR FCC matrix lattice parameters increase with Cr content such that the stoichiometry is ordered 1.8 > 2.0 > 2.2 > 2.4 in agreement with Vegard's law and past works [6], [10], [14], [27]–[29]. As the Fe content increases the FCC matrix lattice parameters increase across each of the AR alloys, as observed in past work [6]. The hardness of the AR alloy softens with higher Fe contents. The change in hardness and starting Vickers hardness show good agreement with previous literature [9], [14], [29]. The lattice contraction quantified via XRD here agree with previous findings [4], [6], [10], [30], [31], that report 0.25% lattice contraction as the saturation value in near stoichiometric (Ni/Cr = 2.0) alloys. The precipitate sizes reported agree with previous TEM observations of LRO Ni_2Cr precipitates from a (Ni/Cr=2.0) sample isothermally aged at 475 °C [10]. The precipitate sizes reported here also agree with results in [14].

The FCC lattice parameter contracts upon aging at all temperatures. In general, the amount of contraction increases with aging temperature (*i.e.,* 475 > 418 > 360 >330 °C). This trend does not hold for alloys containing 7 wt. % Fe or for the hypo-stoichiometric alloy A (Ni-Cr=1.8 + 0 Fe). In both cases, we believe this is due to a lowering of the critical temperature for LRO formation.

The intensity and shape of the Ni_2Cr XRD peaks vary with time, temperature, and composition XRD peak broadening for the Ni_2Cr precipitates at lower temperatures and shorter time periods has previously been observed [10], [14]. The lower intensity and broad peaks are due to the low weight fractions and small precipitate sizes. In our previous research, the phase fraction of Ni_2Cr reaches a maximum value after 500 h at 475 °C for (Ni/Cr=1.8, 2.0, 2.2, 2.4) stoichiometries and plateau at a value of 9 % [10], [14]. This suggests the phase fraction is insensitive to temperature and composition, within the range of Ni/Cr ratios investigated. Therefore, we adopt the conclusion that the phase fraction saturates after early aging times and use the 9 % value proposed in [14] for our XRD refinements and in further analysis of LRO Ni_2Cr.

4.2. Critical resolved shear stress as function of Fe content

To explore the structure-property relationship in Ni-Cr-Fe model alloys we directly compare changes in hardness with Ni_2Cr precipitate size. In binary Ni-Cr model alloys, a linear correlation between the change in hardness and Ni_2Cr precipitate was previously quantified [14]. A critical resolved shear stress

(CRSS) model [14] was found to be effective in describing the increase in hardness with increasing Ni_2Cr precipitate size. CRSS models are commonly applied to describe weak or strong coupled dislocations cutting or shearing through precipitates [32]–[35]. Here, we extend the use of the same CRSS model to understand the role Fe has in the increase in hardness.

In equation (1), τ_{CRSS}, is the critical resolved shear stress, Γ is the anti-phase boundary energy, b is the burger's vector, d is the precipitate diameter (Ni_2Cr precipitate size), f is the volume fraction, and T is the line tension of the dislocation. The line tension is calculated from equation (2) [32], where G is the shear modulus. The shear modulus, G, is calculated from equation (3), where E is the modulus of elasticity, and ν is Poisson's ratio. The numerical factor, A, describes the morphology of precipitates and is 0.72, based on the assumption the Ni_2Cr precipitates are spherical [36].

$$\Delta\tau_{CRSS} = \frac{1}{2}\left(\frac{\Gamma}{b}\right)^{\frac{3}{2}}\left(\frac{bdf}{T}\right)^{\frac{1}{2}}A - \frac{1}{2}\left(\frac{\Gamma}{b}\right)f \quad (1)$$

$$T = \frac{1}{2}Gb^2 \quad (2)$$

$$G = \frac{1}{2}\frac{E}{(1+\nu)} \quad (3)$$

$$\Delta HardnessValue = 3\sqrt{3}\tau_{CRSS} \quad (4)$$

This model, and the linear relationship found between hardness and yield strength [9] combine to predict the hardness from the estimated CRSS as a function of the precipitate size. This is shown in equation (4) where Tabor's relationship [37] and Von Mises flow rule [38] are used to calculate the yield strength from the CRSS, as demonstrated in previous research to calculate the change in hardness [14], [33], [37]–[39]. We report the values used for these equations in Table 3.

Table 3. Model values from this study use the CRSS precipitate hardening model of weakly coupled dislocations to describe Ni_2Cr precipitation.

Parameter	Unit	Model Value	Note
Γ	Jm^{-2}	0.139	Molecular dynamics of model alloy [11]
b	nm	0.254	Ni-based commercial alloy [33], [36]
f	%	9	Ni-Cr model alloy [14]
E	MPa	221	Ni-based commercial alloy [34], [40]
ν	-	0.35	Ni-based commercial alloy [34]
A	-	0.72	Ni-based commercial alloy [36]
d	nm	varies	This work

The CRSS model is shown as a solid gray line in Figure 6. The model shows good agreement with the experimental measurements in capturing both the change in hardness and precipitate size in the Ni-Cr-Fe model alloys investigated here. Figure 6 also includes the previous binary Ni-Cr model alloy LRO Ni_2Cr data shown as small solid magenta circles [14]. The effectiveness of the CRSS model provides further evidence that the size of Ni_2Cr precipitates has notable impacts on the mechanical properties of both Ni-Cr and Ni-Cr-Fe alloys up to 7 wt. % Fe. These results show that LRO Ni_2Cr will likely continue to change

the material property outside of the changes observed in this research. This assertion assumes that the size of the precipitates will continue to grow with increasing aging times. Here the CRSS model predicts that increased precipitate size will continue to harden the material. The model predicts that around the size of 40 nm that the deformation mode will change from precipitate shearing to the classical Orowon or looping mechanism. However, this is only an estimate based on extrapolating the precipitate sizes.

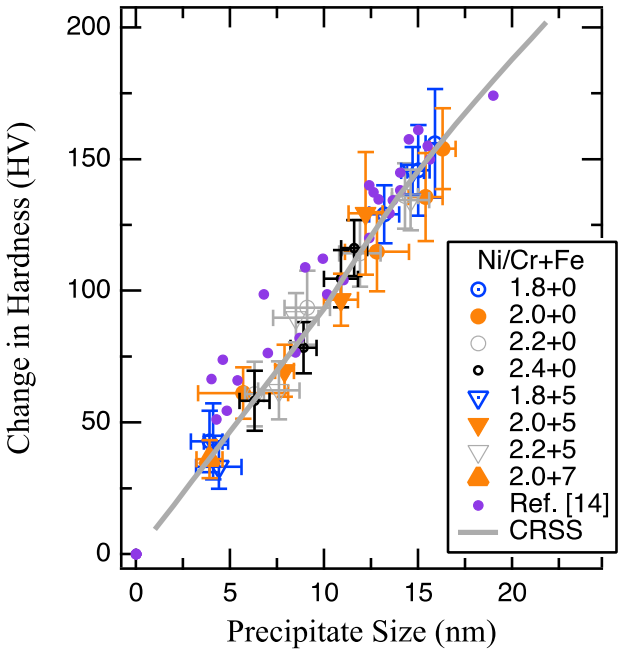

Figure 6 – The precipitate size of LRO Ni_2Cr versus the change in hardness. The solid gray line shows the critical resolved shears stress precipitation hardening model of weakly coupled dislocations.

As we have shown in Figure 6, the fundamental mechanism of thermally induced changes in the mechanical properties of ternary Ni-Cr-Fe alloys is identical to that for the binary Ni-Cr alloys. The formation of Ni_2Cr precipitates in the ternary alloys studied here are hardening centers and pin dislocations. This is abundantly clear from the linear correlation of hardness and Ni_2Cr precipitate size. While minor alloying elements in commercial alloys can trap vacancies and stem the formation of Ni_2Cr [41] (shifting the onset of the formation and growth of Ni_2Cr precipitates), the mechanism by which dislocations are pinned by precipitates does not change. This relationship is a critical step in understanding the differences in LRO formation and evolution between binary, ternary and commercial Ni-based alloys. The results presented here, including the CRSS model, have applications in predicting hardening in commercial alloys, like Alloy 690, whose major components are Ni, Cr, and Fe. The CRSS model described here could be leveraged in future kinetic analysis of Ni_2Cr in commercial alloys where the mechanical performance and material property degradation after long term exposure to elevated thermal environments can be better understood based on the average Ni_2Cr precipitate size.

5. Conclusion

The formation and evolution of long-range ordering was investigated in 11 Ni-Cr-Fe model alloys with 0, 5, 7, and 10 wt. % Fe, after isothermal aging up to 10,000 h at temperatures between 330-475 °C.

The alloys were characterized by hardness and XRD to quantify the impact of Ni_2Cr precipitate size on mechanical properties as a function of Fe content. After 10,000 h at 418°C and 475 °C, the formation of Ni_2Cr was observed in 0 and 5 Fe wt. % alloys. After 10,000 h at 418°C, the same is found with the addition of the alloy G (Ni/Cr=2.0+7 Fe). No clear evidence of Ni_2Cr was observed in any of the 10 wt. % Fe samples at any temperature. No body-centered cubic Cr was observed in any samples. We found that the change in FCC matrix lattice contraction and hardness value both agree with qualitative signs of Ni_2Cr observed in synchrotron XRD patterns. The greatest change in general occurs in stoichiometric alloys with 0 wt. % Fe at 475 °C. The rate of change for 5 wt. % Fe alloys for all stoichiometries is reduced, however the magnitude is similar to 0 wt. % Fe alloys depending on the temperature. The alloy G (Ni/Cr=2.0+ 7 Fe) shows the greatest change at 418 °C, providing evidence that increased Fe lowers the critical temperature. In the off-stoichiometric alloys, we find that the hypo-stoichiometric alloy A (Ni/Cr = 1.8 + 0 Fe) also shows the greatest change at 418 °C. This suggests that increased Cr in these alloys also can significantly decrease critical temperature.

We find that a precipitation hardening model for critical resolved shear stress with weakly coupled dislocations shows good agreement with the material property changes quantified from experimental measurements. Notably finding that the Fe containing alloys are well described by the model. Our results highlight that changes in hardness correlate linearly with Ni_2Cr precipitate size regardless of Fe content to 5 wt. %. To understand if the model fits higher Fe contents, additional isothermal aging time is required. However, the limited data from alloy G (Ni/Cr=2.0) with 7 wt. % Fe is captured with the model. This important structure-property relationship can potentially help define Ni-Cr-Fe-based component lifetimes directly through an understanding of how Ni_2Cr formation impacts strength and ductility as a function of Fe content. These findings highlight the importance of using advanced characterization techniques sensitive to the minor phase populations and capable of quantifying microstructure to assist complex material observations and decisions.

Credit authorship contribution statement

N. J. Aerne: Methodology, Formal analysis, Investigation, Data curation, Writing – original draft, Visualization. **D. J. Sprouster:** Validation, Formal analysis, Investigation, Data curation, Writing – review & editing, Supervision. **J. D. Tucker:** Conceptualization, Methodology, Writing – review & editing, Project administration, Funding acquisition

Declaration of competing interest

The authors declare that they have no known competing financial interests or personal relationships that could have appeared to influence the work reported in this paper.

Data availability

The data will be made available upon request.

Acknowledgements

The authors wish to acknowledge the work of the following individuals for their contribution to this research. Mr. Thomas Wood for his assistance with polishing samples and hardness measurements, Dr. Paul Jablonski and Dr. Martin Detrois at NETL for their help in fabricating and processing the alloy ingots, and Dr. Luanne Rolly for her role in the management of the isothermal aging treatments and furnace system

at Advanced Technology and Manufacturing Institute. Part of this research was conducted at the Northwest Nanotechnology Infrastructure, a National Nanotechnology Coordinated Infrastructure site at Oregon State University which is supported in part by the National Science Foundation (grant NNCI-2025489) and Oregon State University. This research is being supported by the National Science Foundation under Grant no. 1653123-DMR. This publication is also based upon work previously supported by DOE Office of Nuclear Energy's Nuclear Energy University Program, Cooperative Agreement Number DE-NE0008423. This research used resources at the Pair Distribution Function Beamline of the National Synchrotron Light Source II, a U.S. Department of Energy (DOE) Office of Science User Facility operated for the DOE Office of Science by Brookhaven National Laboratory under Contract No. DE-SC0012704.

References

[1] S. J. Zinkle and G. S. Was, "Materials challenges in nuclear energy," *Acta Mater*, vol. 61, no. 3, pp. 735–758, Feb. 2013, doi: 10.1016/j.actamat.2012.11.004.

[2] F. Delabrouille, D. Renaud, F. Vaillant, and J. Massoud, "Long range ordering of Alloy 690," in *14th international conference on environmental degradation of materials in nuclear power system water-reactors, Virginia Beach, Virginia*, 2009.

[3] S. Kim, "Order-disorder reaction in Ni2Cr alloy," in *Transactions of the Korean Nuclear Society Autumn Meeting Gyeongju, Korea*, 2009.

[4] G. A. Young and D. R. Eno, "Long range ordering in model Ni-Cr-X alloys," in *Proceedings of the International Symposium Fontevraud*, 2014, pp. 14–18.

[5] R. Mouginot *et al.*, "Thermal ageing and short-range ordering of Alloy 690 between 350 and 550 °C," *Journal of Nuclear Materials*, vol. 485, pp. 56–66, Mar. 2017, doi: 10.1016/j.jnucmat.2016.12.031.

[6] A. Marucco, "Atomic ordering in the Ni□Cr□Fe system," *Materials Science and Engineering: A*, vol. 189, no. 1–2, pp. 267–276, 1994.

[7] A. Marucco, "A Phase transformations during long-term ageing of Ni-Fe-Cr alloys in the temperature range 450-600 °C," 1995.

[8] B. Stephan, D. Jacob, F. Delabrouille, and L. Legras, "A kinetic study of order-disorder transition in Ni–Cr based alloys," in *Minerals, Metals and Materials Series*, Springer International Publishing, 2018, pp. 233–249. doi: 10.1007/978-3-319-67244-1_15.

[9] G. A. Young, J. D. Tucker, and D. R. Eno, "The kinetics of long range ordering in Ni-Cr and Ni-Cr-Fe alloys," in *Proceedings of the 16th Annual Conference on the Environmentally Assisted Cracking of Materials in Nuclear Power Systems-Water Reactors*, 2013, pp. 1–22.

[10] F. Teng, D. J. Sprouster, G. A. Young, J.-H. Ke, and J. D. Tucker, "Effect of stoichiometry on the evolution of thermally annealed long-range ordering in Ni–Cr alloys," *Materialia (Oxf)*, vol. 8, p. 100453, Dec. 2019, doi: 10.1016/j.mtla.2019.100453.

[11] H. T. Vo *et al.*, "Deformation twinning versus slip in Ni-based alloys, containing Pt2Mo-structured, Ni2Cr-typed precipitates," *Mater Des*, vol. 207, Sep. 2021, doi: 10.1016/j.matdes.2021.109820.

[12] W. Xiong, *Thermodynamic and kinetic investigation of the Fe-Cr-Ni system driven by engineering applications*. Industrial Engineering and Management, Royal Institute of Technology (KTH), 2012.

[13] L. Hao, A. Ruban, and W. Xiong, "CALPHAD modeling based on Gibbs energy functions from zero kevin and improved magnetic model: A case study on the Cr–Ni system," *CALPHAD*, vol. 73, Jun. 2021, doi: 10.1016/j.calphad.2021.102268.

[14] N. Aerne, D. J. Sprouster, and J. D. Tucker, "The formation and evolution of Ni2Cr precipitates in Ni–Cr model alloys as a function of stoichiometry characterized by synchrotron x-ray diffraction," *Materials Science and Engineering A*, vol. 856, Oct. 2022, doi: 10.1016/j.msea.2022.143930.

[15] E. Frely, “Study of the interactions between irradiation and chemical order effects in ternary alloys Ni-Cr-Fe,” CEA Saclay, 1997.
[16] M. Song, Y. Yang, M. Wang, W. Kuang, C. R. Lear, and G. S. Was, “Probing long-range ordering in nickel-base alloys with proton irradiation,” *Acta Mater*, vol. 156, pp. 446–462, Sep. 2018, doi: 10.1016/j.actamat.2018.06.043.
[17] P. D. Jablonski and C. J. Cowen, “Homogenizing a nickel-based superalloy: thermodynamic and kinetic simulation and experimental results,” *Metallurgical and Materials Transactions B*, vol. 40, no. 2, pp. 182–186, 2009.
[18] P. D. Jablonski and J. A. Hawk, “Homogenizing advanced alloys: thermodynamic and kinetic simulations followed by experimental results,” *J Mater Eng Perform*, vol. 26, no. 1, pp. 4–13, 2017.
[19] H. Abrams, “Grain size measurement by the intercept method,” *Metallography*, vol. 4, no. 1, pp. 59–78, 1971.
[20] E.-96 ASTM, “Standard test methods for determining average grain size,” *ASTM International: West Conshohocken, PA, USA*, 2004.
[21] J. M. Schneider, M. Bigerelle, and A. Iost, “Statistical analysis of the Vickers hardness,” *Materials Science and Engineering A*, vol. 262, no. 1–2, pp. 256–263, Apr. 1999, doi: 10.1016/s0921-5093(98)01000-4.
[22] X. Shi, S. Ghose, and E. Dooryhee, “Performance calculations of the X-ray powder diffraction beamline at NSLS-II,” *J Synchrotron Radiat*, vol. 20, no. 2, pp. 234–242, 2013.
[23] D. J. Sprouster *et al.*, “Advanced synchrotron characterization techniques for fusion materials science,” *Journal of Nuclear Materials*, vol. 543, Jan. 2021, doi: 10.1016/j.jnucmat.2020.152574.
[24] J. Ilavsky, “Nika: software for two-dimensional data reduction,” *J Appl Crystallogr*, vol. 45, no. 2, pp. 324–328, 2012.
[25] J. Ilavsky and P. R. Jemian, “Irena: tool suite for modeling and analysis of small-angle scattering,” *J Appl Crystallogr*, vol. 42, no. 2, pp. 347–353, 2009.
[26] L. Lutterotti, M. Bortolotti, G. Ischia, I. Lonardelli, and H.-R. Wenk, “Rietveld texture analysis from diffraction images,” in *Tenth European Powder Diffraction Conference*, Oldenbourg Wissenschaftsverlag, 2015, pp. 125–130.
[27] J. D. Tucker, “AB INITIO-BASED MODELING OF RADIATION EFFECTS IN THE NI-FE-CR SYSTEM,” 2008.
[28] L. Vegard, “Die konstitution der mischkristalle und die raumfüllung der atome,” *Zeitschrift für Physik*, vol. 5, no. 1, pp. 17–26, 1921.
[29] A. Verma, J. B. Singh, S. D. Kaushik, and V. Siruguri, “Lattice parameter variation and its effect on precipitation behaviour of ordered Ni2(Cr,Mo) phase in Ni-Cr-Mo alloys,” *J Alloys Compd*, vol. 813, Jan. 2020, doi: 10.1016/j.jallcom.2019.152195.
[30] P. Nash, “Phase diagrams of binary nickel alloys,” *ASM International(USA), 1991,* p. 394, 1991.
[31] B. Gwalani *et al.*, “Experimental investigation of the ordering pathway in a Ni-33 at.% Cr alloy,” *Acta Mater*, vol. 115, pp. 372–384, 2016.
[32] L. M. Brown and R. K. Ham, “Strengthening methods in crystals,” *Applied Science, London*, vol. 9, 1971.
[33] Q. Wang, Z. Li, S. Pang, X. Li, C. Dong, and P. K. Liaw, “Coherent precipitation and strengthening in compositionally complex alloys: A review,” *Entropy*, vol. 20, no. 11. MDPI AG, Nov. 01, 2018. doi: 10.3390/e20110878.
[34] J. H. Oh, I. C. Choi, Y. J. Kim, B. G. Yoo, and J. il Jang, “Variations in overall- and phase-hardness of a new Ni-based superalloy during isothermal aging,” *Materials Science and Engineering A*, vol. 528, no. 19–20, pp. 6121–6127, Jul. 2011, doi: 10.1016/j.msea.2011.03.115.
[35] J. Moon, S. Kim, J. il Jang, J. Lee, and C. Lee, “Orowan strengthening effect on the nanoindentation hardness of the ferrite matrix in microalloyed steels,” *Materials Science and Engineering A*, vol. 487, no. 1–2, pp. 552–557, Jul. 2008, doi: 10.1016/j.msea.2007.10.046.

[36] B. Reppich, “Some new aspects concerning particle hardening mechanisms in γ’ precipitating Ni-base alloys—I. Theoretical concept,” *Acta Metallurgica*, vol. 30, no. 1, pp. 87–94, Jan. 1982, doi: 10.1016/0001-6160(82)90048-7.
[37] D. Tabor, “A simple theory of static and dynamic hardness,” *Proc R Soc Lond A Math Phys Sci*, vol. 192, no. 1029, pp. 247–274, 1948.
[38] R. v Mises, “Mechanik der festen Körper im plastisch-deformablen Zustand,” *Nachrichten von der Gesellschaft der Wissenschaften zu Göttingen, Mathematisch-Physikalische Klasse*, vol. 1913, pp. 582–592, 1913.
[39] P. Zhang, S. X. Li, and Z. F. Zhang, “General relationship between strength and hardness,” *Materials Science and Engineering A*, vol. 529, no. 1, pp. 62–73, Nov. 2011, doi: 10.1016/j.msea.2011.08.061.
[40] J. James, J. Julian, J. Rahul, G. Philip, J. Devassy, and P. Reba, “Effect of recasting on physical properties of base metal alloys: An in vitro study,” *J Int Soc Prev Community Dent*, vol. 8, no. 5, p. 457, 2018, doi: 10.4103/jispcd.jispcd_237_18.
[41] J. D. Tucker, “Solute-vacancy interactions in nickel,” *MRS Online Proceedings Library*, vol. 1645, pp. 1–6, 2014.